

Emergence of localized in-gap states in conjugated polymers of branched topology

Shiyong Wang, Weihua Wang, and Nian Lin*

Department of Physics, The Hong Kong University of Science and Technology, Hong Kong, China

(Received 23 April 2012; revised manuscript received 30 May 2012; published 18 July 2012)

Using cryogenic scanning tunneling microscopy and spectroscopy, we investigated cross-linked phenylene-based polymers with various branched morphology at a single-molecule resolution. We found that localized states that are in the band gap of un-branched polymers emerge at the branch junctions. These in-gap states can be shifted close to the Fermi level through three means: extending the length of branch arms, coupling adjacent branches in hyperbranched structures, or increasing the number of branch arms. Single-band tight-binding calculations can reproduce all experimental results and provide quantitative relationships between the energy level shifts and the branching geometry. Our discovery evidences the emergence and development of in-gap states in the band structures of conjugated systems with fractional dimensions.

DOI: [10.1103/PhysRevB.86.045428](https://doi.org/10.1103/PhysRevB.86.045428)

PACS number(s): 73.61.Ph, 68.37.Ef, 73.22.-f, 82.35.Cd

I. INTRODUCTION

Carbon-based aromatic systems provide a unique platform for studying electronic structure as well as charge transport in different dimensions.^{1,2} At one extreme, benzene can be viewed as a zero-dimensional object which has a wide gap between its occupied and unoccupied states. The other extreme is two-dimensional (2D) gapless graphene. Between the two extremes, there exist a large variety of structures exhibiting rich properties, including fullerenes, polycyclic aromatic hydrocarbon molecules, one-dimensional (1D) aromatic polymers,³ nanoribbons,⁴ nanotubes, and porous graphene.² In this wide spectrum, hyperbranched structures show a fractal topology and represent a transition state from 1D polymers to 2D graphene. Electronic excitation in these structures can be spatially delocalized or localized depending on the branching topology.⁵ Thus, unraveling the electronic states of the hyperbranched polymers may shed lights on the band structure development of π -electron systems from the gapped 1D polymers to the gapless 2D graphene.

Hyperbranched polymers and dendrimers have been synthesized in polymer chemistry and extensively used in technological applications due to their interesting electronic properties.^{6,7} Experimental measurements evidenced that hyperbranched topology red-shifts the absorption peak⁷ significantly, enhances the conductivity and controls the direction of electron flow.^{2,8} Hyperbranched systems have also been addressed theoretically. For example, it was predicated that addition of several side branches at a molecule wire produces a noticeable increase in electron transfer rates;⁹ branched topologies show conductance higher than the linear chain counterparts due to the increase in the band width due to the additional side groups,¹⁰ and the connectivity in branched polymers may lead to localization of the electronic states even within the “bands”.¹¹ Particularly interesting is that these structures are proposed to be used as monomolecular electronic circuits,¹² such as single-molecule transistors, quantum-interference devices, and spin filters.^{13–15} However, the electronic structures of hyperbranched conjugated polymers have not yet been explored experimentally at a single-molecule level and many theoretical predications could not be tested directly. In this paper, we report on a systematic study on single conjugated oligomers with branched topology.

Using scanning tunneling microscopy (STM) and tunneling spectroscopy (STS) working at 5 K, we discovered that the branches introduce new unoccupied electronic states that lie below the lowest-unoccupied molecular orbital (LUMO), that is, in the band gap, of the unbranched oligomers. Furthermore, we found that the energy level of these in-gap states depends on the length of branch arms, the coupling of neighboring branches in hyperbranched structures, as well as the number of branch arms of multiarm structures. These observations demonstrate that the branched aromatic polymers exhibit electronic characteristics in between the gapped 1D polymers and the gapless 2D graphene. Our results illustrate a progressive evolution of the electronic band structures of the carbon-based aromatic systems in terms of dimensionality.

II. EXPERIMENT AND CALCULATION

The experiments were carried out in a commercial STM system (Omicron) operated at cryogenic temperature (4.9 K) and ultrahigh vacuum condition ($\sim 10^{-11}$ mbar). A single crystal Cu(111) sample was cleaned by cycles of Ar⁺ sputtering and annealing to ~ 900 K. The precursor molecules were thermally evaporated onto Cu(111) substrate held at room temperature and followed a >470 K annealing to form conjugated structures. The STM topographic data were acquired in constant current mode. The differential tunneling spectroscopic (dI/dV) data were acquired using a lock-in amplifier with a sine modulation of 1.5 kHz at 15 mV. The dI/dV scans along the molecules were measured at constant tunneling set point. In the local density of states (LDOS) maps, each spectrum is normalized by dividing I/V .

The precursor molecule is 4,4'-dibromo-*p*-terphenyl, which contains two Br atoms at the two terminals of a *p*-terphenylene as shown in Fig. 1(b). On the Cu(111) surface, debromination occurs at 300 K catalyzed by Cu adatoms and, at >470 K, polyphenylene (PP) oligomers are formed.^{16–18} At higher annealing temperatures, in addition to the chainlike oligomers, many branched structures are present, as marked by the red circles in Fig. 1(a). The branched topology is formed via dehydrogenation of the phenylene moieties. As illustrated in Figs. 1(b) and 1(c), two types of three-arm branches, Y-shaped and star-shaped, are formed with a different reaction site.

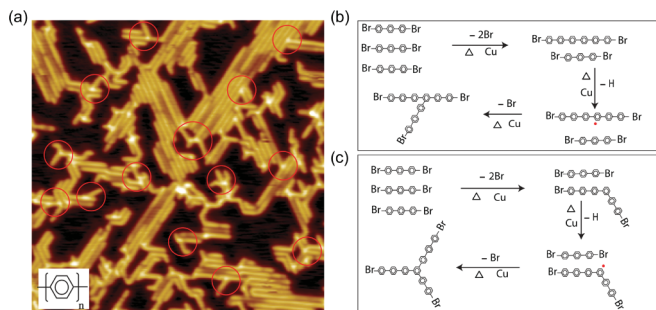


FIG. 1. (Color online) (a) STM image ($60 \times 60 \text{ nm}^2$; 1.0 V, 0.5 nA) showing PP (inset model) oligomers. The red circles mark several branched structures. [(b) and (c)] Reaction path of forming a Y-shaped and a star-shaped three-arm branch, where dehydrogenation of a phenylene moiety, as marked by the red dots, occurs as an intermediate step.

Single-band tight binding (TB) calculations were carried out considering nearest-neighbor hopping.¹⁶ Following the notation of the inset in Fig. 3(c), the Hamiltonian is expressed as

$$H = E_0 \sum_n^{i+j+k+1} c_n^\dagger c_n - t \sum_n^{i,j,k} [c_{n+1}^\dagger c_n + c_n^\dagger c_{n+1}] - t \sum_e [c_e^\dagger c_0 + c_0^\dagger c_e], \quad (1)$$

where E_0 is the on-site energy and t the nearest-neighbor hopping integral. The third term corresponds to the hopping at the branch junction, where site 0 denotes the central phenyl unit of the branch junction and sites e denote the end phenyl units of the three branch arms that connect the central phenyl unit. The same on-site energy E_0 (2.9 eV) and the nearest-neighbor hopping integral t (1.15 eV) were used in all TB calculations. In the TB calculations, a Gaussian function was used to simulate the energy broadening (spatial broadening) with a standard variance of 0.2 eV (2 Å).

III. RESULTS AND DISCUSSION

Figures 2(a)–2(d) show close views of four typical branched structures and the corresponding structural models: Figure 2(a) shows a Y-shaped three-arm branch, Fig. 2(b) shows a star-shaped three-arm branch, Fig. 2(c) shows a hyperbranched structure which contains two three-arm branches linked via

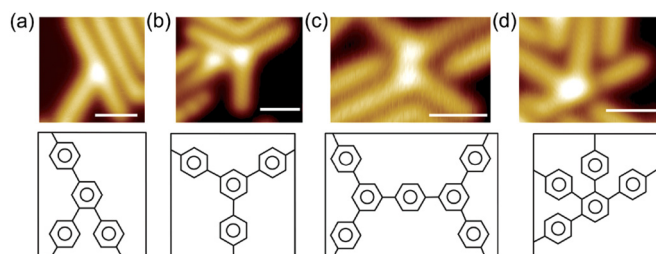


FIG. 2. (Color online) Close-view STM images and molecular models of (a) a Y-shaped three-arm branch, (b) a star-shaped three-arm branch, (c) a hyperbranched structure, and (d) a four-arm branch. 1.0 V, 0.5 nA; all scale bars = 2 nm.

a spacer, and Fig. 2(d) shows a four-arm branch. Notably, the apparent height of the branch junction sites (imaged at 1.0 V bias) is always higher than the rest of the oligomers. As indicated by the STM topograph acquired at -0.1 V imaging condition, the branch junctions are at a similar adsorption height as the rest parts. Thus, the enhanced apparent height in the 1.0 V images cannot be attributed to geometric effects but rather caused by additional electronic states localized at the branch junctions. In the following, we will present detailed investigations of the local electronic states of different branch structures.

A. Three-arm branches

We measured differential tunneling spectra (dI/dV) along the dashed lines in Figs. 3(a)–3(d) point by point. The obtained dI/dV spectra are expressed as condensed LDOS maps as shown in the up panels of Figs. 3(e)–3(h).^{16,17} In these maps, the horizontal axis refers to the positions along the dashed lines in Figs. 3(a)–3(d), the vertical axis refers to energy defined with bias voltage (the positive energy corresponds to state above Fermi level, i.e., unoccupied states), and the color refers to the LDOS intensity. Our previous study reported that straight or kinked PP oligomers have appreciate LDOS at energy above 0.8 eV, revealing that the LUMO of the straight or kinked oligomers lies at 0.8 eV above the Fermi level.¹⁶ In contrast, Figs. 3(e)–3(h) clearly shows that new states below 0.8 eV appear at the branch junctions [hence, the new states are denoted as branch junction state (BJS)]. As these new states are below 0.8 eV, we conclude the branched topology creates in-gap states that are localized at the branch junctions. Note the Y-shaped and the star-shaped three-arm branches exhibit no significant difference. It is worthwhile to point out that similar bound state was detected at the junction of two intersecting quantum wells in a T-shaped GaAs/AlGaAs system.¹⁹ Recently, Fölsch *et al.* reported that Y-shaped branched adatom chains exhibit similar localized low-lying states.²⁰ It is interesting that the localized low-lying states

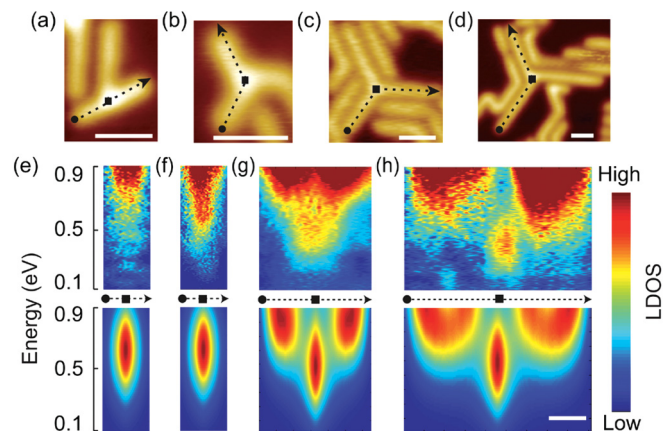


FIG. 3. (Color online) (a) STM image of a Y-shaped three-arm branch. [(b)–(d)] STM images (1.0 V, 0.5 nA) showing three star-shaped three-arm branches with different arm length. [(e)–(h)] (Upper panels) LDOS maps of tunneling spectra measured along the dashed lines in (a)–(c), respectively; (lower panels) TB calculated LDOS along the dashed lines. All scale bars = 2 nm.

appear as a common characteristic for the atomic, molecular, and semiconductor branched structures. However, the kinked atom chains exhibit a localized lower-lying state; while, in contrast, the kinked PP chains do not show the low-lying states.¹⁶ We will discuss this difference later. The lower panels in Figs. 3(e)–3(h) show the TB calculated LDOS maps. The calculated results exhibit a spatially localized state below the LUMO of the unbranched oligomers and the energy level agrees very well with the experimental results. Kopelman *et al.* reported that the lowest-energy band excitations are localized at the nodes of branched structures based on the comparison of the electronic spectra of a family of compact dendrimers.²¹ Our results directly reveal the electronic localization at the branch junctions.

Figure 3(b)–3(d) shows three star-shaped symmetric three-arm branches of different sizes (each has three equally long arms consisting of three, six, and nine phenyl units in Figs. 3(b), 3(c), and 3(d), respectively). The corresponding LDOS maps clearly show that the BJS appears at 0.6 eV [Fig. 3(f)], 0.4 eV [Fig. 3(g)], and 0.3 eV [Fig. 3(h)], respectively, revealing a downshift of BJS to Fermi level as the branch arm length increases. This experimentally resolved downshift of BJS energy level (E_{BJS}) is reproduced in the TB calculated results as well [cf. the low panels in Figs. 3(f)–3(h)]. The downshift of E_{BJS} as a function of branch arm length n of four symmetric branches (the total size of the branch $N = 3n + 1$) is plotted in Fig. 4(a). As reported previously, LUMO level of straight PP oligomers scales with $1/N$ (N refers to the size of the oligomers).¹⁶ However, E_{BJS} exhibits a different dependence on the branch's size: It decreases sharply as the branch's size increases up to $N = 19$ ($n = 6$) and then approaches a saturation value of 0.45 eV for larger N . This different downshift trend can be attributed to the localization of the BJS, that is, the BJS is localized around the branch junction within about five phenyl units so E_{BJS} is insensitive to further increment of the branch arms when the arms are longer than five phenyl units; in contrast, in straight PP oligomers the LUMO states are delocalized, which gives rise to the $1/N$ scaling of the LUMO level.

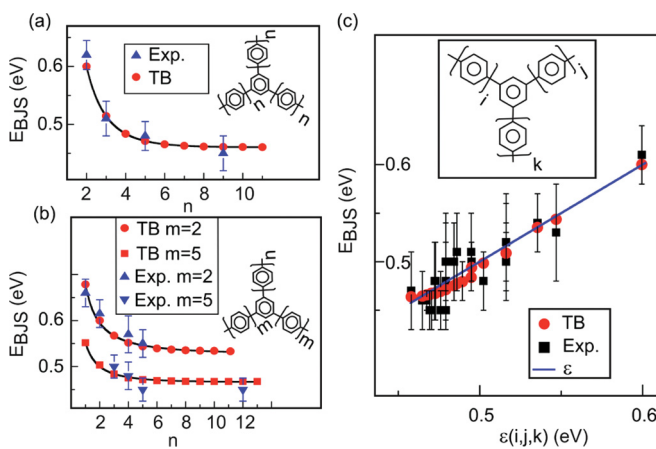


FIG. 4. (Color online) [(a) and (b)] Experimentally measured and TB calculated energy levels of the BJS (E_{BJS}) plotted versus the number of units n , where n is defined in the inset. (c) Energy levels of the BJS plotted versus the coupling function $\epsilon(i,j,k)$, where i, j , and k are the number of units in each arm as defined in the inset.

In addition to the symmetric three-arm branches, we have investigated totally 27 three-arm branches of various arm length, including asymmetric arms. All these samples exhibit in-gap BJS and their energy level E_{BJS} depends on the branch arm length as well. In general, the longer the arms are, the lower the E_{BJS} is. This result is consistent with an early report that dendrimers of similar structure but different molecular branches' lengths exhibit a decrease in the band edge energy with a growing size of the system.²¹ Figure 4(b) shows E_{BJS} of the three-arm branches that contain two equally long (denoted by m) arms depending on the length of the third branch arm (denoted by n). For two serials of $m = 2$ and $m = 5$, E_{BJS} shows the same shift trend as shown in Fig. 4(a). Interestingly, for $m = 2$ serial, even the third arm is very long ($n = 10$), E_{BJS} can only approach to 0.55 eV, i.e., 0.1 eV higher than the saturation value shown in Fig. 4(a). This observation hints that E_{BJS} depends not only on the total size of a branched oligomer but more on the length of its shortest arm. Thus, for a three-arm branch with two long arms and one short arm, E_{BJS} is more sensitive to the length of the short arm rather than the long ones. As for asymmetric branches the dependence of E_{BJS} on the branch arms' length shows a more complex behavior, here we define a coupling function $\epsilon(i,j,k)$ to describe the shifting trend of E_{BJS} in terms of the arm length of three branches:

$$\begin{aligned} \epsilon(i,j,k) = & \delta + \alpha \sum_{n=i,j,k} \varphi(n) + \beta^2 \sum_{n,m=i,j,k}^{n=m} \varphi(n)\varphi(m) \\ & + \gamma^3 \prod_{n=i,j,k} \varphi(n), \end{aligned} \quad (2)$$

where i, j, k stand for the length of the three arms, respectively, and

$$\varphi(n) = \frac{\sin\left(\frac{\pi}{2(n+2)}\right)}{n+1}.$$

In function $\varphi(n)$, $n+1$ defines the length of individual branch arms including the central phenyl unit, and the sine function represents the intensity of the LUMO wave function at the end of the branch arm given the arm is isolated from the branch junction. The second term in Eq. (2) accounts for the contribution of individual branch arms to BJS (note the LUMO level of a straight oligomer is scaled with its length as $1/N$).¹⁶ The third and the fourth terms account for the contribution of the two-arm coupling and the three-arm coupling at the branch junction, respectively, to the BJS.

The measured as well as the TB calculated BJS energy levels E_{BJS} of all branches are plotted as a function of the coupling function $\epsilon(i,j,k)$ in Fig. 4(c) with $\delta = 0.44$ eV, $\alpha = 0.31$ eV, $\beta^2 = 0.6$ eV, and $\gamma^3 = 14$ eV [the blue line represents $\epsilon(i,j,k)$]. One can see the coupling function $\epsilon(i,j,k)$ reproduces the general shifting trend of the experimentally observed as well the TB calculated E_{BJS} fairly well. In the coupling function, the first term δ (0.44 eV) defines the limit of the E_{BJS} downshifting. The nonzero δ indicates that there always exists an energy gap at the branch junction regardless how long the arms are. The second term gives rise to the observed behavior that E_{BJS} of a branch junction with two long arms and one short arm is more sensitive to the length of the short arm. The

coefficient of the three-arm coupling is larger than that of the two-arm coupling ($\gamma > \beta$) implies that the three-arm coupling plays more significant roles than the two-arm coupling in constructing the BJS. In other words, the observed BJS is a characteristic feature of the branch topology but not of the kinked topology. This effect explains the absence of detectable BJS in the kinked structures because the kinked structures only have a weak two-arm coupling term.¹⁶

B. Hyperbranched structures

Next, we have investigated the hyperbranched structures to probe electronic coupling of neighboring BJS. Here, to exclude the effects of E_{BJS} dependence on arm length, we choose the hyperbranched structures that contain branches with two long arms (larger than 10 phenyl units) since E_{BJS} of these branches only depends on the shortest arm [cf. Fig. 4(b)]. Figures 5(a)–5(c) shows three hyperbranched structures, each containing two adjacent branch junctions linked by a spacer group. The size of the spacer group is defined by the number of phenyl unit n as illustrated by the molecular model in Fig. 5(g). In Figs. 5(d)–5(f), the up panels display the experimentally acquired and the low panels display the TB calculated LDOS maps along the dashed lines in Figs. 5(a)–5(c), respectively. As $n = 3$, the LDOS maps [Fig. 5(d)] show a ~ 0.5 eV state distributed at the spacer. As $n = 1$, the spacer is reduced to one phenyl unit, the LDOS maps [Fig. 5(e)] show a ~ 0.35 eV state localized at the spacer. In an extreme case of $n = 0$ while the two branches are connected by a C-C single bond, the LDOS maps [Fig. 5(f)] show a ~ 0.3 eV state localized at the single bond. In all three cases, the energy levels of the new states are lower than those of the individual component three-arm branches. We attribute the new states to an effective electronic coupling of the two BJS of the component branches via the spacer group.²² To quantitatively analyze the coupling effect, we define an energy reduction as $\Delta E = E_1 + E_2 - 2E_h$, where E_1 and E_2 stand for the energy levels of the BJS of the two component three-arm branches and E_h the energy level of the hyperbranched structure.

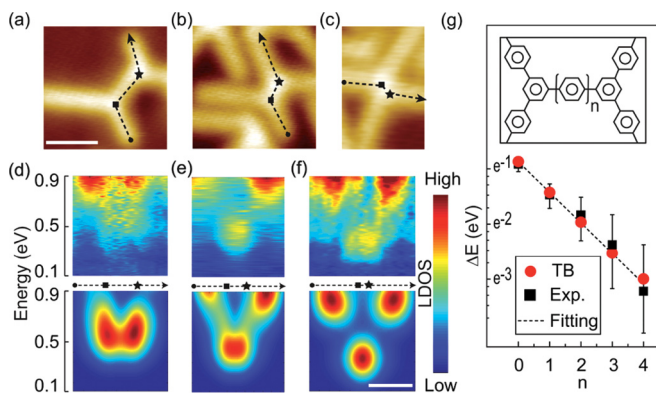


FIG. 5. (Color online) [(a)–(c)] STM images (1.0 V, 0.5 nA; all in same scale) showing hyperbranched structures with different spacers: (a) $n = 3$, (b) $n = 1$, and (c) $n = 0$ [n is defined in the inset of (g)]. [(d)–(f)] (Upper panels) LDOS maps of tunneling spectra measured along the dashed lines in (a)–(c), respectively; (lower panels) TB calculated LDOS along the dashed lines. (g) Energy reduction ΔE plotted as a function of spacer size (n). All scale bars = 2 nm.

Figure 5(g) shows the experimentally measured and the TB calculated ΔE as a function of spacer size n . One can see ΔE decays exponentially with increasing spacer size, obeying a relationship of $\Delta E = A \exp(-\beta d)$, where $d = (4.3n + 1.3)$ Å, stands for the length of the spacer group. Fitting of the data results in a decay constant $\beta = 0.12$ Å⁻¹. This decay constant is very close to the value (0.10 Å⁻¹) obtained previously in similar polyphenylene systems.²²

C. Multiarm branches

In addition to the three-arm branches, we have investigated various multiarm branches. Figure 6(a) shows a four-arm branch and Fig. 6(b) a five-arm branch. These multiarm branches also exhibit localized BJS states. Figures 6(c) and 6(d) reveal the BJS of the four-arm (five-arm) branch is at ~ 0.35 eV (~ 0.3 eV). Figure 6(e) displays E_{BJS} of the multiarm branches of three-arm, four-arm, and five-arm branches as a function of the number of branch arms (as a reference the LUMO of the unbranched straight PP polymer denoted as No. = 2 is also shown). The wide range of E_{BJS} dependence on the branch arm length as discussed previously. Despite the wide range, the downshift of the E_{BJS} with increasing number of branch arms is obvious. This trend is reproduced by the TB calculations of different multiarm branches (with arms of 12 units) shown by the red dots in Fig. 6(f). The calculated results can be quantitatively summarized as $\Delta E_n = -0.25n$ eV + 0.46 eV, where $\Delta E_n = E_n - E_2$, E_n refers to E_{BJS} of the n -arm branch structure and E_2 the LUMO level of the straight PP polymer. This relation infers that addition of one arm at a branch junction may down shift the BJS state by 0.25 eV. In the case that the band structures of electron and hole are symmetric, this downshifting results in a band gap narrowing of 0.5 eV. We have not observed six-arm branches experimentally. Nevertheless, it is worthwhile to note that, taking into account straight PP polymers have a band gap of 2.8–3.1 eV,^{23,24} a six-arm branch may have a very narrow gap or even gapless BJS state.

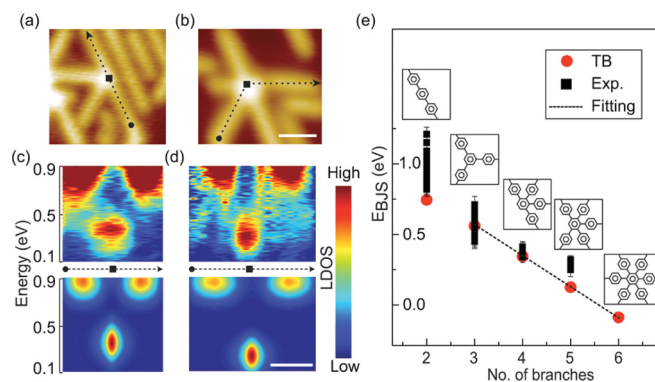


FIG. 6. (Color online) [(a) and (b)] STM images (1.0 V, 0.5 nA) showing (a) a four-arm branch and (b) a five-arm branch. [(c) and (d)] (Upper panel) LDOS maps of tunneling spectra measured along the dashed lines in (a) and (b), respectively; (lower panels) TB calculated LDOS along the dashed lines. (e) E_{BJS} of the multibranch structures plotted as a function of number of branch arms. All scale bars = 2 nm.

IV. CONCLUSIONS

In conclusion, we found that branch junctions of polyphenylene oligomers introduce localized states that lie in the gap of the unbranched polymers. We established quantitative relationships between the energy level of these in-gap states and the underlying branched structures, including branch arm length, hyperbranched structures, and multiarm structures.

These results afford insight into the narrowing of band gap and the enhancement of conductivity of conjugated polymers with branched topology.

ACKNOWLEDGMENT

This work is supported by the Hong Kong RGC (Grant No. 603611).

*Corresponding author: phnlin@ust.hk

- ¹F. Chen and N. J. Tao, *Acc. Chem. Res.* **42**, 573 (2009).
- ²M. Terrones, A. R. Botello-Méndez, J. Campos-Delgado, F. López-Urías, Y. I. Vega-Cantú, F. J. Rodríguez-Macías, A. L. Elías, E. Muñoz-Sandoval, A. G. Cano-Márquez, J.-C. Charlier, and H. Terrones, *Nano Today* **5**, 351 (2010).
- ³A. J. Heeger, *Rev. Mod. Phys.* **73**, 681 (2001).
- ⁴Y.-W. Son, M. L. Cohen, and S. G. Louie, *Phys. Rev. Lett.* **97**, 216803 (2006).
- ⁵C. Wu, S. V. Malinin, S. Tretiak, and V. Y. Chernyak, *Nat. Phys.* **2**, 631 (2006).
- ⁶S. M. Grayson and J. M. J. Frechet, *Chem. Rev.* **101**, 3819 (2001).
- ⁷C. Gao and D. Yan, *Prog. Polym. Sci.* **29**, 183 (2004).
- ⁸G. Zotti, R. Salmaso, M. C. Gallazzi, and R. A. Marin, *Chem. Mater.* **9**, 791 (1997).
- ⁹T. S. Elicker, J. S. Binette, and D. G. Evans, *J. Phys. Chem. B* **105**, 370 (2001).
- ¹⁰C. Kalyanaraman and D. G. Evans, *Nano Lett.* **2**, 437 (2002).
- ¹¹S. M. Risser, D. N. Beratan, and J. N. Onuchic, *J. Phys. Chem.* **97**, 4523 (1993).
- ¹²C. Joachim, J. K. Gimzewski, and A. Aviram, *Nature* **408**, 541 (2000).

- ¹³A. S. R. Botello-Méndez, E. Cruz-Silva, J. M. Romo-Herrera, F. López-Urías, M. Terrones, B. G. Sumpter, H. Terrones, J.-C. Charlier, and V. Meunier, *Nano Lett.* **11**, 3058 (2011).
- ¹⁴G. C. Solomon, D. Q. Andrews, R. H. Goldsmith, T. Hansen, M. R. Wasielewski, R. P. Van Duyne, and M. A. Ratner, *J. Am. Chem. Soc.* **130**, 17301 (2008).
- ¹⁵A. A. Kocherzhenko, L. D. A. Siebbeles, and F. C. Grozema, *J. Phys. Chem. Lett.* **2**, 1753 (2011).
- ¹⁶S. Y. Wang, W. H. Wang, and N. Lin, *Phys. Rev. Lett.* **106**, 206803 (2011).
- ¹⁷S. Wang, W. Wang, and N. Lin, *ACS Nano* **6**, 3401 (2012).
- ¹⁸W. Wang, X. Shi, S. Wang, M. A. Van Hove, and N. Lin, *J. Am. Chem. Soc.* **133**, 13264 (2011).
- ¹⁹L. N. Pfeiffer, K. W. West, A. Pinczuk, H. U. Baranger, and H. L. Stormer, *Appl. Phys. Lett.* **61**, 1956 (1992).
- ²⁰J. Lagoute, X. Liu, and S. Fölsch, *Phys. Rev. B* **74**, 125410 (2006).
- ²¹R. Kopelman, M. Shortreed, Z. Y. Shi, W. Tan, Z. Xu, J. S. Moore, A. Bar-Haim, and J. Klafter, *Phys. Rev. Lett.* **78**, 1239 (1997).
- ²²W. H. Wang, S. Y. Wang, X. Y. Li, J. P. Collin, J. Liu, P. N. Liu, and N. Lin, *J. Am. Chem. Soc.* **132**, 8774 (2010).
- ²³G. Grem, G. Leditzky, B. Ullrich, and G. Leising, *Adv. Mater.* **4**, 36 (1992).
- ²⁴G. Grem, V. Martin, F. Meghdadi, C. Paar, J. Stampfl, J. Sturm, S. Tasch, and G. Leising, *Synth. Met.* **71**, 2193 (1995).